3/15/95

SANDIA REPORT

SAND95–0311 • UC–705
Unlimited Release
Printed February 1995

On the Feasibility of Using Smoothed Particle Hydrodynamics for Underwater Explosion Calculations

J. W. Swegle, S. W. Attaway

Prepared by
Sandia National Laboratories
Albuquerque, New Mexico 87185 and Livermore, California 94550
for the United States Department of Energy
under Contract DE-AC04-94AL85000

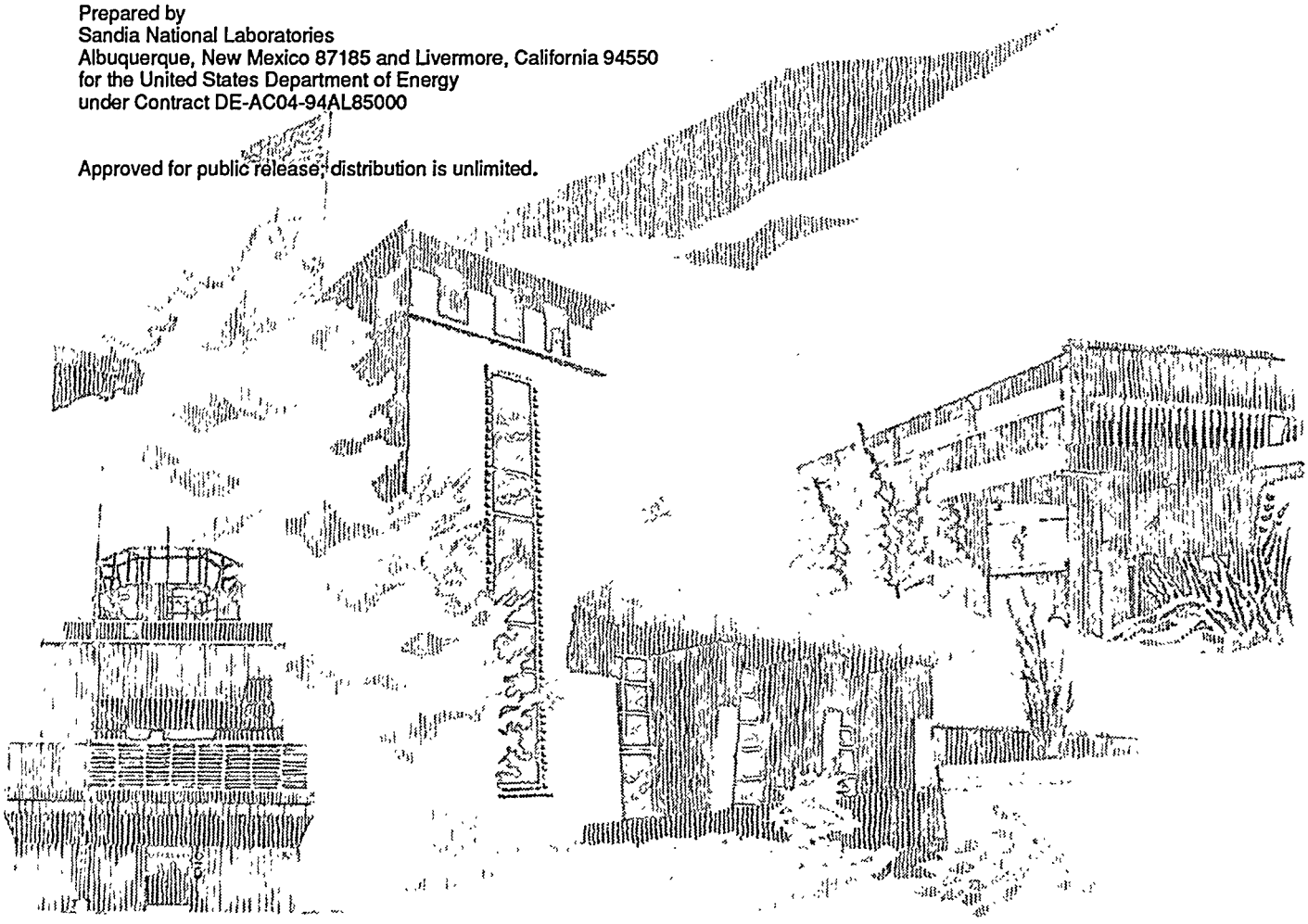

SF2900Q(8-81)

DISCLAIMER

Portions of this document may be illegible in electronic image products. Images are produced from the best available original document.

SAND95-0311
Unlimited Release
Printed February 1995

Distribution
Category UC-705

On the Feasibility of Using Smoothed Particle Hydrodynamics for Underwater Explosion Calculations

J. W. Swegle
S. W. Attaway
Material and Structural Mechanics Department, 1518
Sandia National Laboratories
Albuquerque, New Mexico 87185

Abstract

SPH (Smoothed Particle Hydrodynamics) is a gridless Lagrangian technique which is appealing as a possible alternative to numerical techniques currently used to analyze high deformation impulsive loading events. In the present study, the SPH algorithm has been subjected to detailed testing and analysis to determine the feasibility of using PRONTO/SPH for the analysis of various types of underwater explosion problems involving fluid-structure and shock-structure interactions. Of particular interest are effects of bubble formation and collapse and the permanent deformation of thin walled structures due to these loadings. These are exceptionally difficult problems to model. Past attempts with various types of codes have not been satisfactory. Coupling SPH into the finite element code PRONTO represents a new approach to the problem. Results show that the method is well-suited for transmission of loads from underwater explosions to nearby structures, but the calculation of late time effects due to acceleration of gravity and bubble buoyancy will require additional development, and possibly coupling with implicit or incompressible methods.

This work was performed at Sandia National Laboratories, which is operated for the U. S. Department of Energy under Contract No. DE-AC04-94AL85000, and was partially funded by the Naval Surface Warfare Center under WFO proposal #15930816.

35

Intentionally Left Blank

Contents

Figures

1. Introduction

SPH (Smoothed Particle Hydrodynamics)[1-9] is a gridless Lagrangian technique which is appealing as a possible alternative to numerical techniques currently used to analyze high deformation impulsive loading events, such as hypervelocity impact or explosive loading of materials. While Eulerian techniques can easily handle the gross motions associated with the large deformations involved in such events, detailed analysis is difficult because of the lack of history and the smearing and spreading of information (referred to here as diffusion) as the mass moves through the fixed-in-space Eulerian grid. Standard Lagrangian techniques, although desirable due to their ability to keep accurate histories of the events associated with each Lagrangian element, cannot be used because the material deformations are so large that the Lagrangian grid becomes severely distorted and the calculation breaks down.

SPH offers a possible solution to these difficulties. The technique is Lagrangian and thus provides complete history information and should be well-suited for tracking details of the deformation process associated with each material element. SPH is actually quite similar to standard Lagrangian methods. In fact, the term hydrodynamic in the name is a misnomer, since strength is easily included. The difference from standard techniques is that spatial gradients are approximated by a method which is applicable to an arbitrary distribution of interpolation points so that no grid is required.Thus, the technique is gridless and should be applicable to arbitrary deformations, including the production of individual fragments. The lack of a grid also means that 3D calculations are as easy as 1D. Various organizations which have chosen SPH as a natural technique for large deformation calculations have used it to produce numerous results and are strongly supportive of its capabilities.

SPH has been coupled into the transient dynamics finite element code, PRONTO[10], providing a combined capability which exceeds the individual capabilities of either method. The coupling embeds the SPH method within the finite element code and treats each SPH particle as an different element type within the finite element architecture. Contact surface algorithms used in the finite element method are used to couple the SPH particles with the finite elements. The ability to couple particle methods and finite element method allows fluid-structure interaction problems to be solved efficiently. SPH can be used in large deformation regions where standard Lagrangian finite elements would become too distorted. However, SPH need not be used for the entire problem. Low deformation regions and structures can be treated with finite elements. Also, very thin regions can be treated with shell elements. Since various types of boundary conditions are easier to apply to finite elements than SPH, SPH regions can be surrounded by finite elements for the purpose of applying boundary conditions.

The purpose of the present effort is to evaluate the feasibility of using PRONTO/SPH for the analysis of various types of underwater explosion problems involving fluid-structure and shock-structure interactions. Of particular interest are effects of bubble formation and collapse such as the loads on structures due to bubble pulses and cavitation closure, the formation of re-entrant jets during bubble collapse, the interaction of these jets with a structure, and the permanent deformation of thin walled structures due to these loadings. These are exceptionally difficult problems to model. Past attempts with various types of codes have not been satisfactory. Coupling SPH into the finite element code PRONTO represents a new approach to the problem.

As part of this effort, considerable development work has been done on PRONTO/SPH. SPH has been added to the three-dimensional version of PRONTO, including the latest developments in variable smoothing length, methods for calculating density, as well as interface and smoothing options. Also, an axisymmetric option has been added to the two-dimensional version of PRONTO. Throughout this report, a familiarity with SPH is assumed and no technical details concerning the SPH method are provided. The reader unfamiliar with SPH should consult reference 9 for a description of SPH.

2. Plane Wave on a Spherical Shell

The first test problem involves a plane acoustic wave incident on a hollow spherical elastic shell submerged in water. Analytic solutions are available for the response of the shell[11-12]. The first test involved a pure finite-element calculation using the two-dimensional axisymmetric mesh shown in Figure 2.1. The left boundary is the cylindrical symmetry axis, and a pressure of roughly 20 atmospheres is applied to the top surface. This pressure was chosen to satisfy the acoustic approximation inherent in the analytic solution, and is so small that the relative motion between the water and the shell is essentially negligible during the time of the calculation. The right and bottom boundaries are placed far enough away from the shell that no wave reflections from them reach the shell during the time of the calculation. A close-up view of the mesh in the vicinity of the shell in shown in Figure 2.2. The thickness of the shell is one-fiftieth of its radius, so that the individual elements in the shell cannot be detected. Comparisons of calculated and analytical results for the radial velocity at the top and bottom of the shell are shown in Figure 2.3 for three different mesh resolutions. The coarse, regular, and fine calculations have 20, 50, and 125 elements along the half-circumference of the sphere. The calculations show excellent agreement with the analytic solution.

The second test involved a pure SPH calculation using the initial particle distribution shown in Figure 2.4.The figure shows the initial particle distribution as well as the initial pressure and vertical velocity in the calculation. This is also an axisymmetric calculation with the particles reflected across the symmetry plane to generate the plot. Again, the thickness of the shell is so much less than its radius that individual particles in the shell cannot be detected, although the shell has uniform particle distribution with four particles through the shell thickness. In this calculation no attempt was made to match the positions of the water particles to the shell surface, but rather all particles in the water were placed on a regular lattice. No water particles were placed at a lattice positions which fell inside the outer diameter of the shell, resulting in the steps in the positions of the water particles next to the sphere surface. Although a smoother interface could easily have been constructed, it was of interest to see if this quick, albeit rather crude, placement could yield acceptable results. As shown in Figure 2.5 the agreement between calculated and analytical results is again quite good.

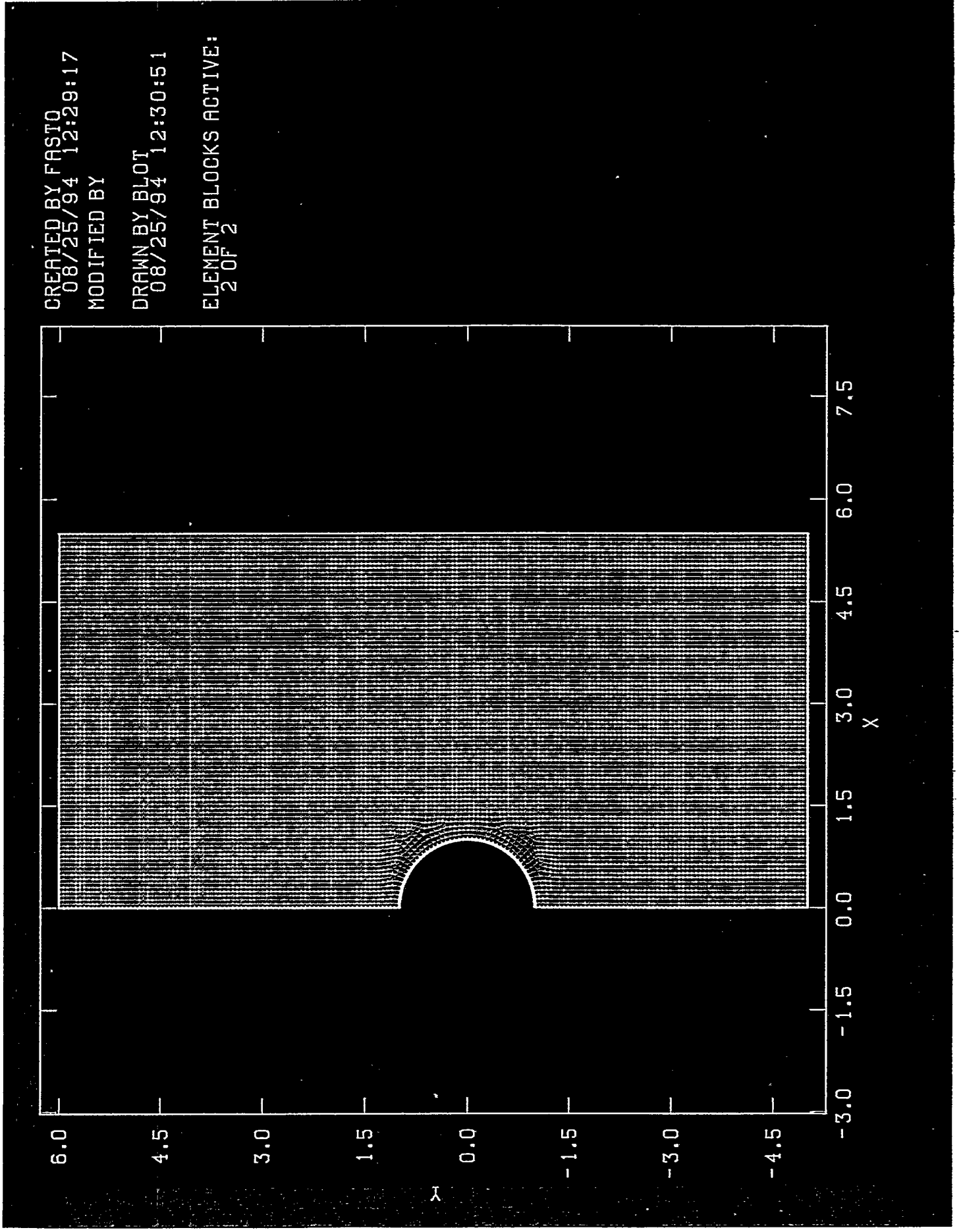

Figure 2.1 Finite element mesh for the submerged sphere problem. Positions are in centimeters.

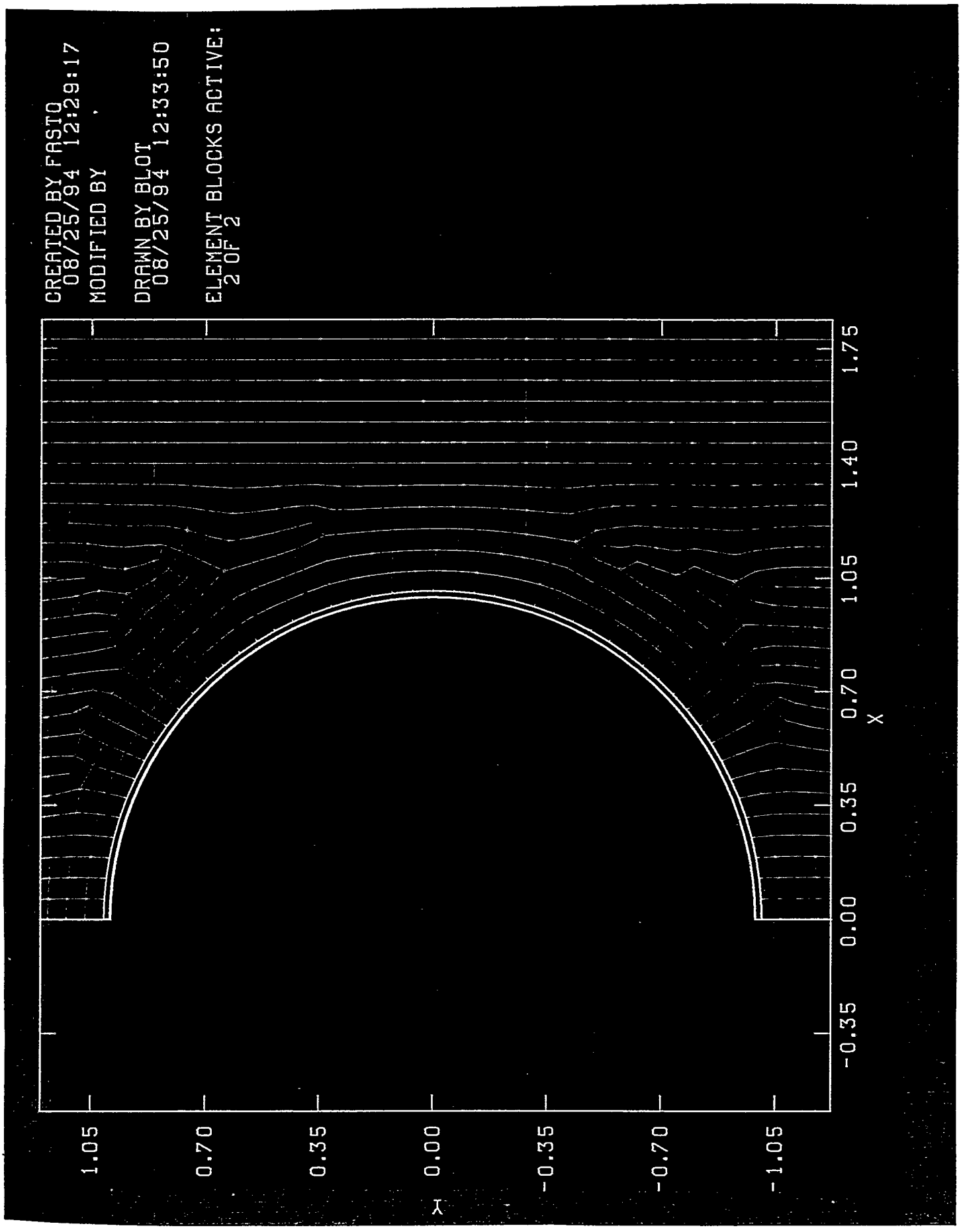

Figure 2.2 Close-up of the finite-element mesh in the vicinity of the spherical shell.

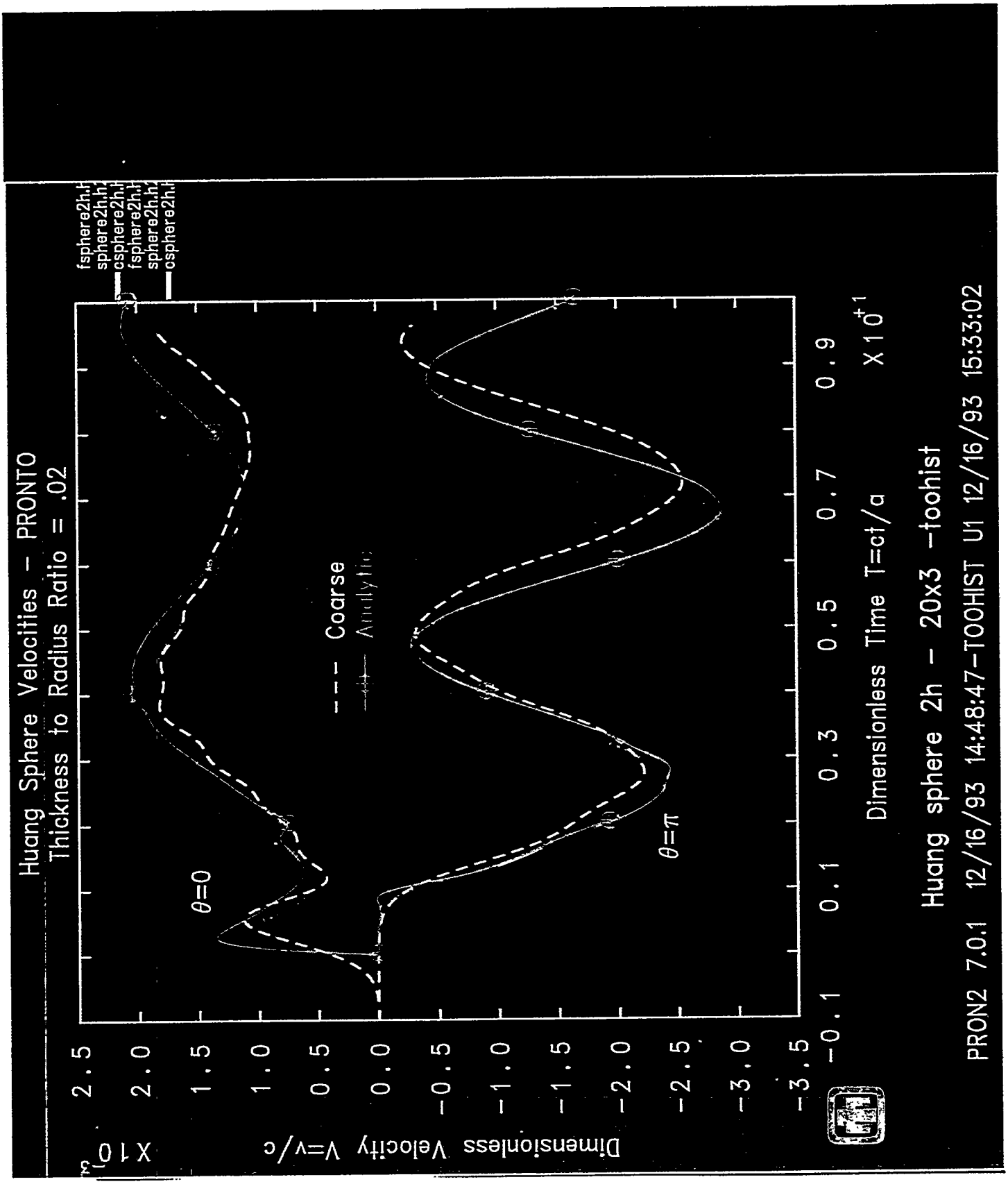

Figure 2.3 Comparison of finite-element and analytical results for the velocity at the top ($\theta = 0$) and bottom ($\theta = \pi$) of the shell. Velocity and time are non-dimensionalized by the sound velocity in the water, c, and the radius, a, of the shell.

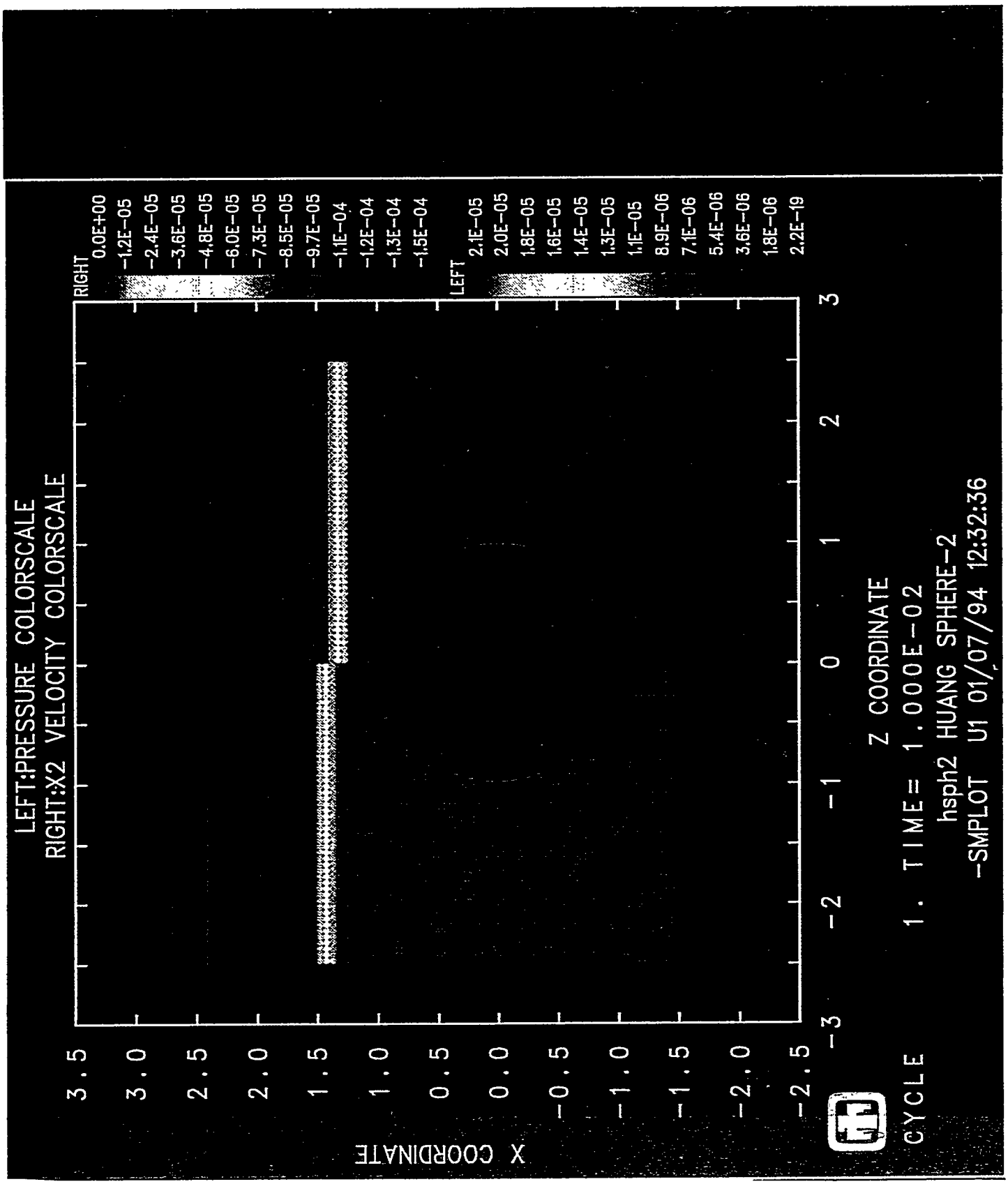

Figure 2.4 Initial conditions for pressure and vertical particle velocity in the SPH calculation of the submerged sphere. Pressure is Mbar and velocity is cm/μsec.

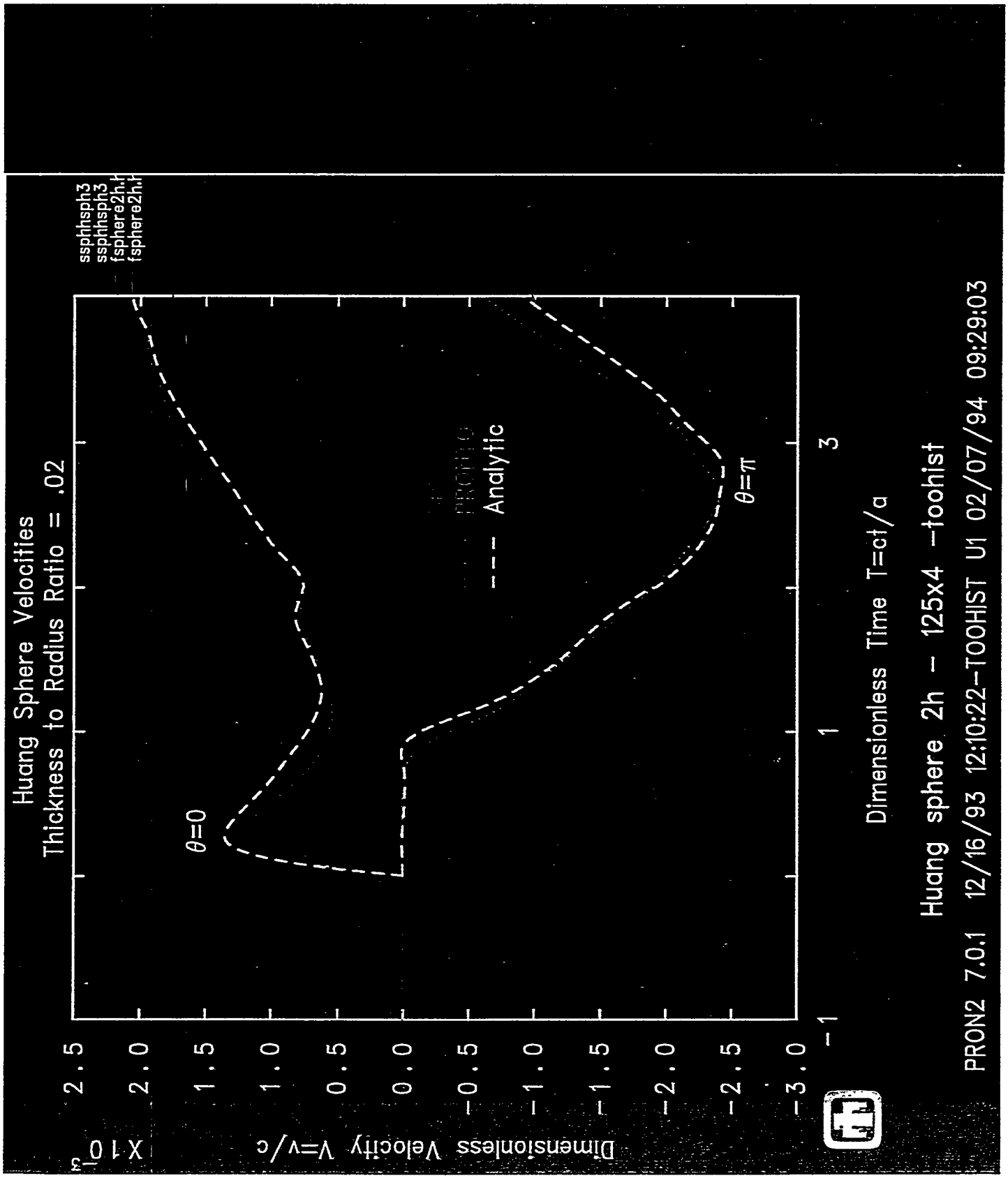

Figure 2.5 Comparison of SPH and analytical results for the radial velocity at the top ($\theta = 0$) and bottom ($\theta = \pi$) of the shell. Velocity and time are non-dimensionalized by the sound velocity in the water, c, and the radius, a, of the shell.

3. Underwater Bubble Period and Radius

The next test was to determine whether pure SPH could correctly predict the first period and maximum radius of the explosive products gas bubble resulting from the underwater detonation of an explosive charge. After detonation of the charge, the rapid expansion of the bubble and the inertia of the outwardly moving water cause the bubble to expand beyond the point of pressure equilibrium. After further expansion the higher pressure in the surrounding water reverses the motion and the bubble contracts. Again, equilibrium is overshot, and at the next minimum of the bubble size the gas is recompressed to several hundred atmospheres. This forms a second 'explosion' and the process is repeated several times. Simple theories have been developed to predict the bubble period and maximum radius[13].

Pure SPH calculations were done to compare bubble period and radius with theory and also with results from other types of numerical methods. Comparison with other calculations is a more direct check of the SPH results than comparison with predictions of the simple theory, since the underlying physics and assumptions involved in the theory may differ from those in the calculations, and a specific calculation using a particular equation of state for the explosive and water may not necessarily agree with the theory. Two different calculations can be set up with identical conditions and material properties so that the only differences should be in the numerical solution methods. The SPH results were compared with results from the Lagrangian finite-difference wavecode TOODY[14]. Although the SPH calculations were two-dimensional and axisymmetric, the deformations are too large for a gridded Lagrangian code, so the TOODY calculations were one-dimensional and spherically symmetric.

In order to keep the bubble period relatively short and to bound the ratio of the maximum bubble radius to the initial explosive radius, calculations were performed for the detonation of 1000 kg of TNT at a depth of 5000 m. The initial pressure in the surrounding water was set to the pressure at this depth, but rather than adding the acceleration of gravity and the variation of pressure with depth, the initial pressure in the water was about 0.5 kbar, independent of depth. Figure 3.1 shows SPH results for particle positions and pressures at times (from left to right and top to bottom) prior to detonation, at first bubble maximum, first bubble minimum, and second bubble maximum. The particles are reflected about the symmetry axis to produce the plot, with the color on the left side of the axis corresponding to type of particle (red for explosive, green for water), and the color on the right corresponding to a pressure color scale (pressure units in Mbar.) The boundaries are reflective and are only a few maximum bubble radii away from the detonation point in order to provide a close-up view of the particles in the gas bubble. The figure emphasizes the adaptive gridding provided by the variable smoothing length option in the SPH method. The explosive particles are initially considerably smaller than the water particles, but as they expand and their density increases, the size of the particle's interaction region increases so that they can keep in

communication. Density in all calculations shown in this report is calculated by the kernel sum method, with boundary anomalies accounted for by multiplying all densities at all times by the ratio of the ambient density to the kernel sum density calculated at time zero.

Figure 3.2 shows a much larger calculation with the boundaries moved far enough away to have negligible effect on the first bubble period and maximum radius. In this calculation the position of the shock at the time of the first bubble maximum is clearly shown (upper right). The initial shock is just reflecting from the boundaries at the time of the first bubble minimum (lower left), and the outgoing pressure pulse produced at that time can clearly be seen interacting with the ingoing waves reflected from the boundary (lower right).

Comparisons of bubble size versus time for the two types of calculations for different mesh resolutions are shown in Figure 3.3. In the figure legend, '2D SPH' refers to the SPH calculations, and '1D VNR' (von-Neumann Richtmyer difference method) refers to the TOODY calculations. As can be seen, resolution has an effect on the calculations. The two methods are in reasonable agreement, even though the SPH calculations are not truly spherically one dimensional. The simple theory predicts a maximum bubble radius of about 2 m, and a first period of about 16 ms, so the calculations are in general agreement with the simple theory, although the two numerical methods agree with each other better than with the theory.

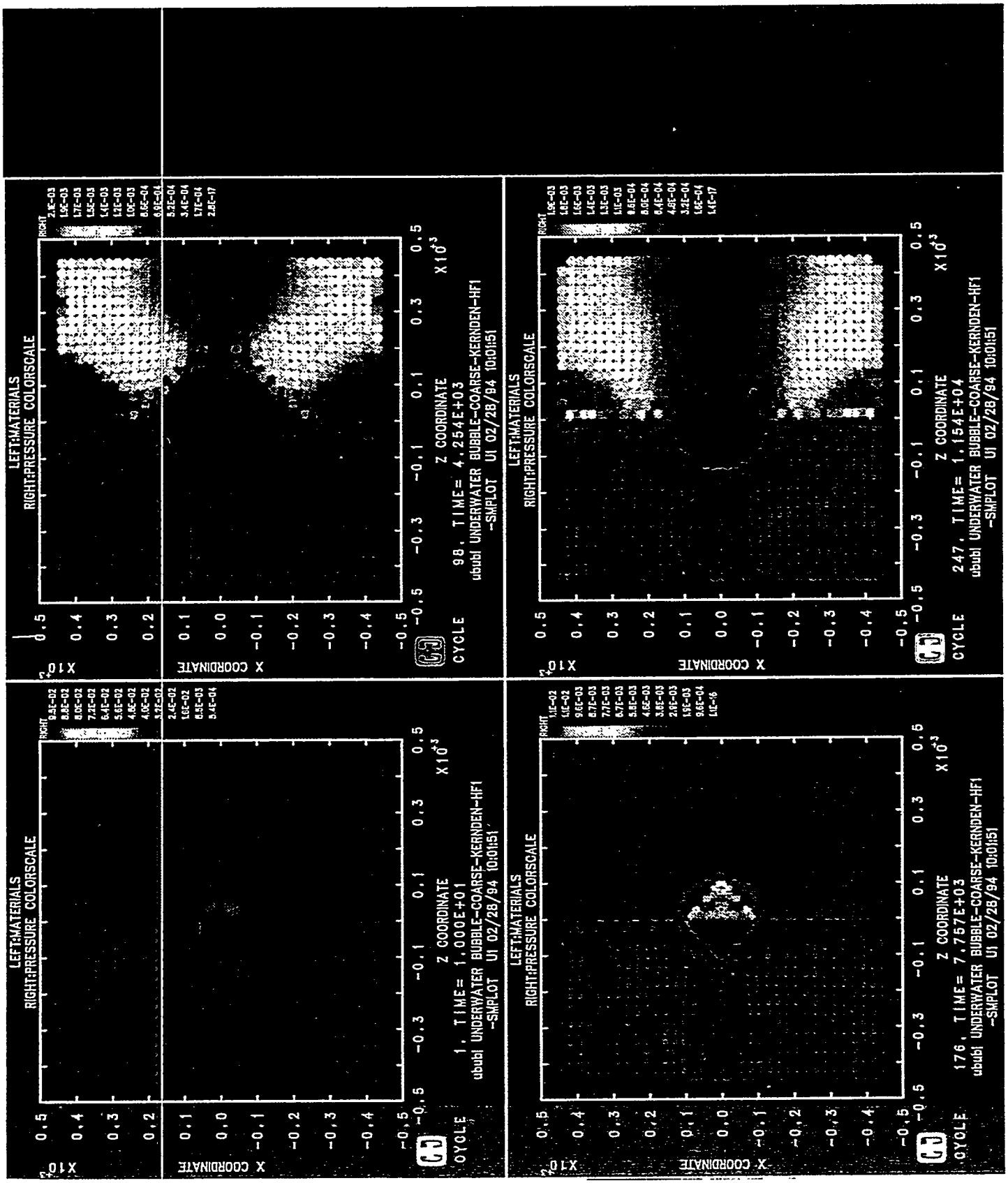

Figure 3.1 Material and pressure plots for an underwater detonation with near boundaries. Pressure in Mbar.

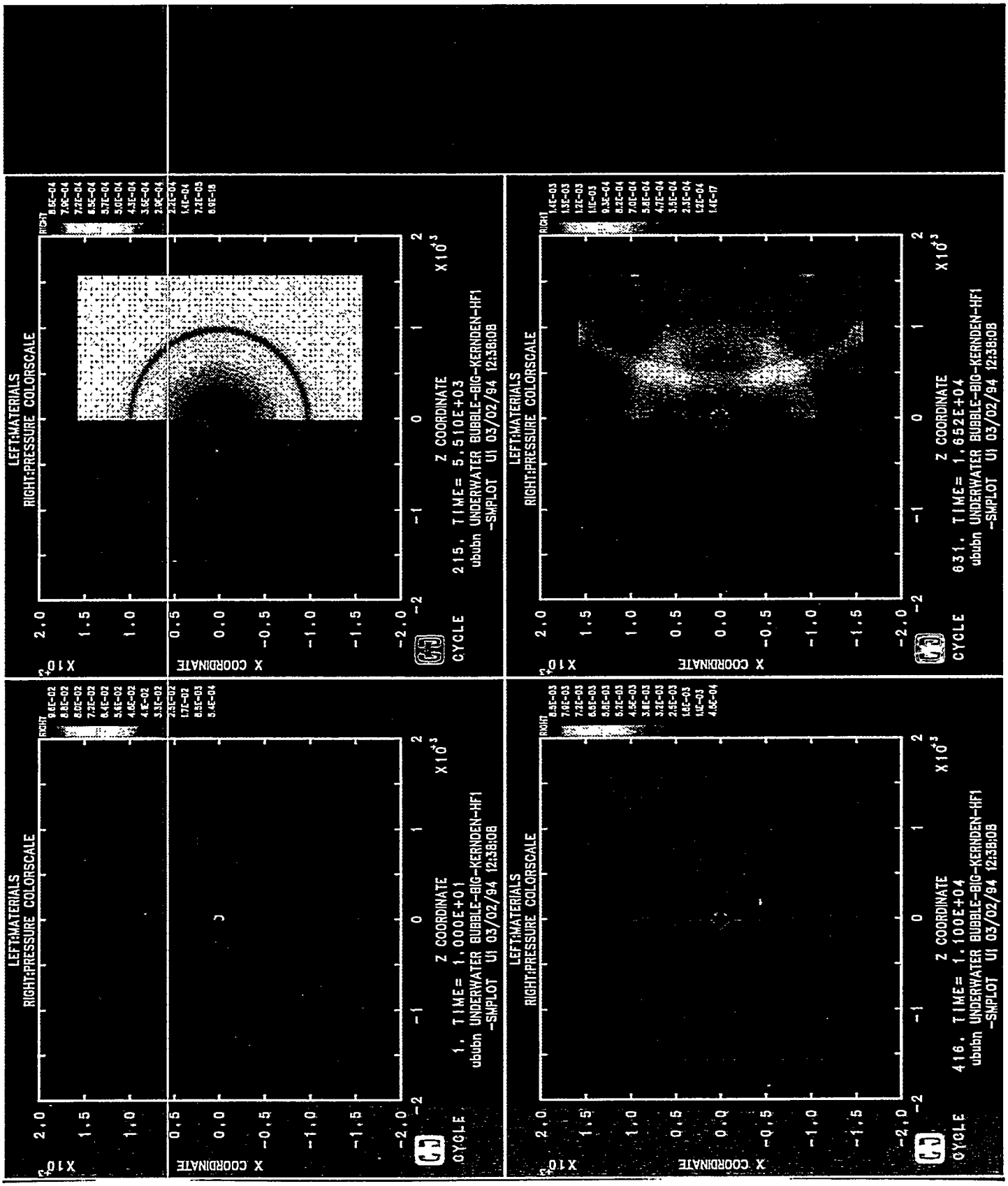

Figure 3.2 Material and pressure plots for an underwater detonation with far boundaries. Pressure in Mbar

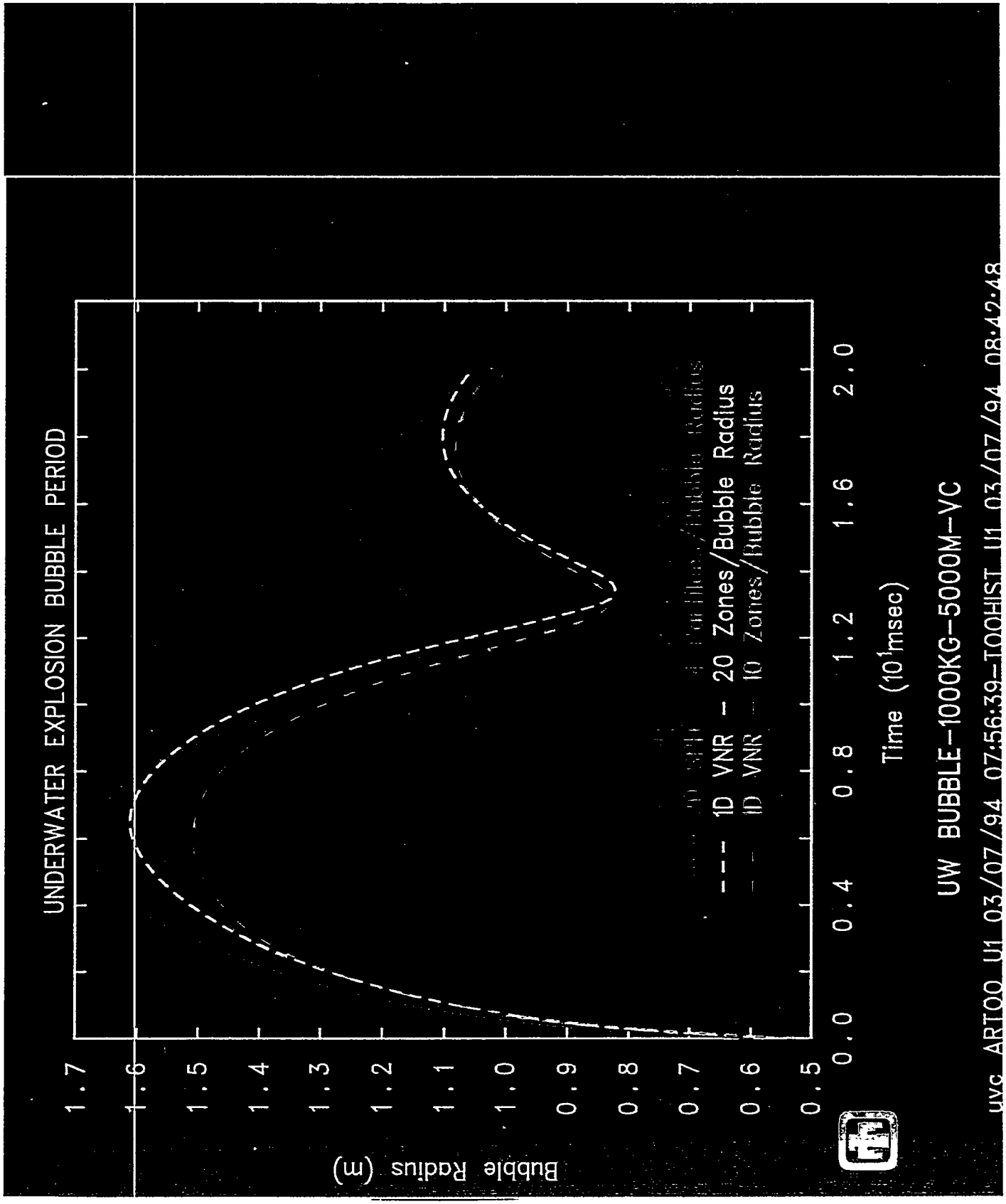

Figure 3.3 Comparison of bubble size histories for 2D axisymmetric SPH calculations and 1D spherically symmetric TOODY (VNR) calculations.

4. Shallow Explosion Above a Hollow Cylinder

The next test involves the detonation of a shallow charge above a thin-walled aluminum pipe. The charge is 15 gm (2 mm/side) of pentolite at a depth of 7 cm, located 9 mm above a 46 cm (18 inch) diameter, 0.48 cm (0.19 inch) wall thickness pipe. The geometry is representative of a series of experiments known as IED cylinder tests[15]. The initial three-dimensional setup of the problem for a 3 foot long section of pipe is shown in Figure 4.1. Gravity was not included and the initial pressure in the water is zero. The calculation demonstrates the full PRONTO capabilities for coupling different types of elements, since the explosive and nearby water are SPH (which is treated as simply another element type in PRONTO), the rest of the water is hex elements, and the pipe is shell elements. A close-up of the SPH region is shown in Figure 4.2, which emphasizes the difference in the initial sizes of the SPH water particles and the SPH explosive particles.

Figure 4.3 shows the propagation of the pressure pulse due to the detonation of the explosive from the SPH region into the surrounding finite-element water. The SPH particles and the shell elements are not shown in this figure. Figure 4.4 shows a series of plots of the material deformation at various times (indicated on the figure in microseconds). Again, the figure emphasizes the adaptive gridding of the variable smoothing length option in the SPH method as the size of the explosive particles increases while their density decreases. Although no quantitative comparisons were made with experiment because of unknowns in the experimental configuration, the calculations agree qualitatively with the deformations observed in the pipe in the tests, and demonstrate the feasibility of using PRONTO/SPH for coupled fluid-structure interactions.

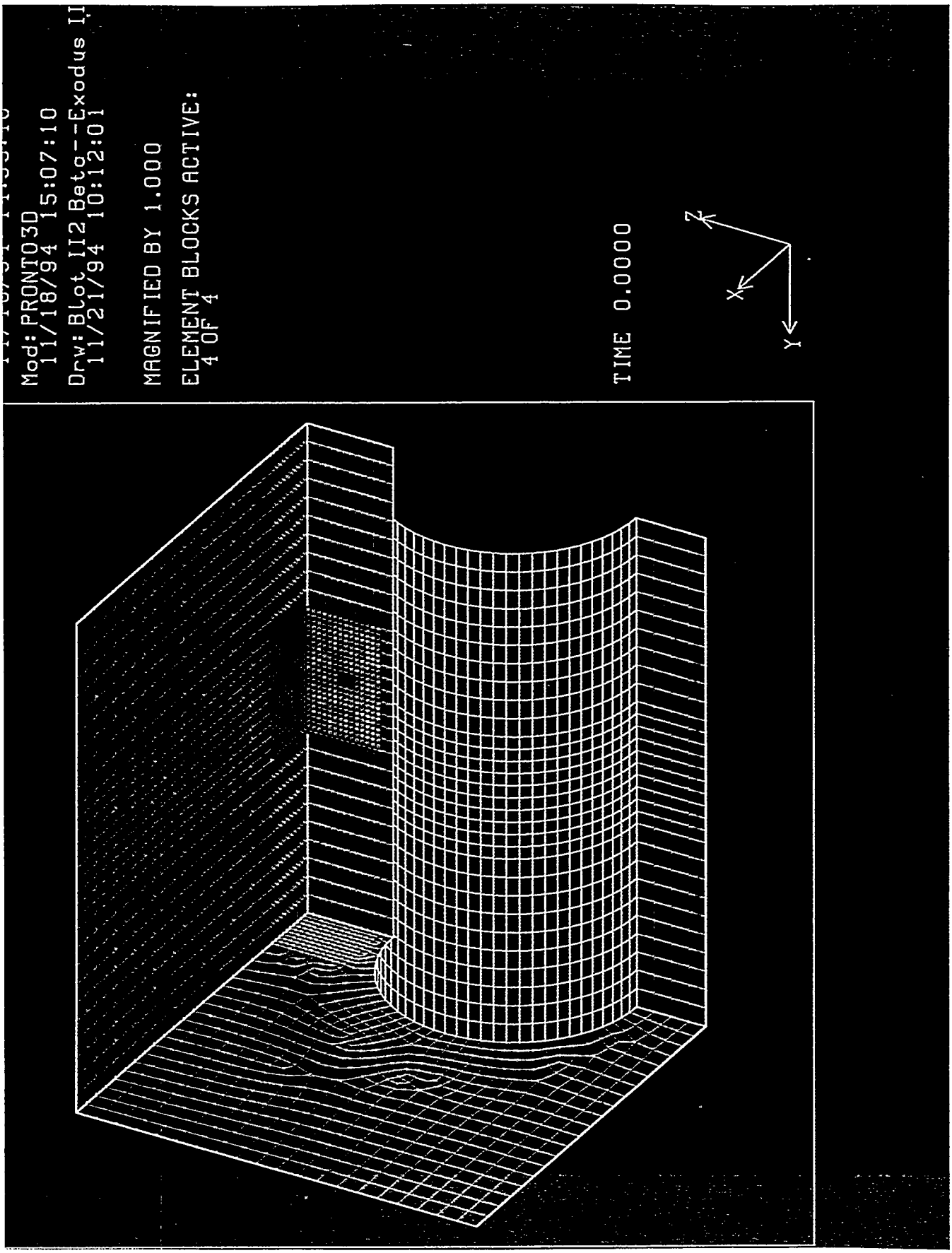

Figure 4.1 Mesh for the submerged cylinder problem.

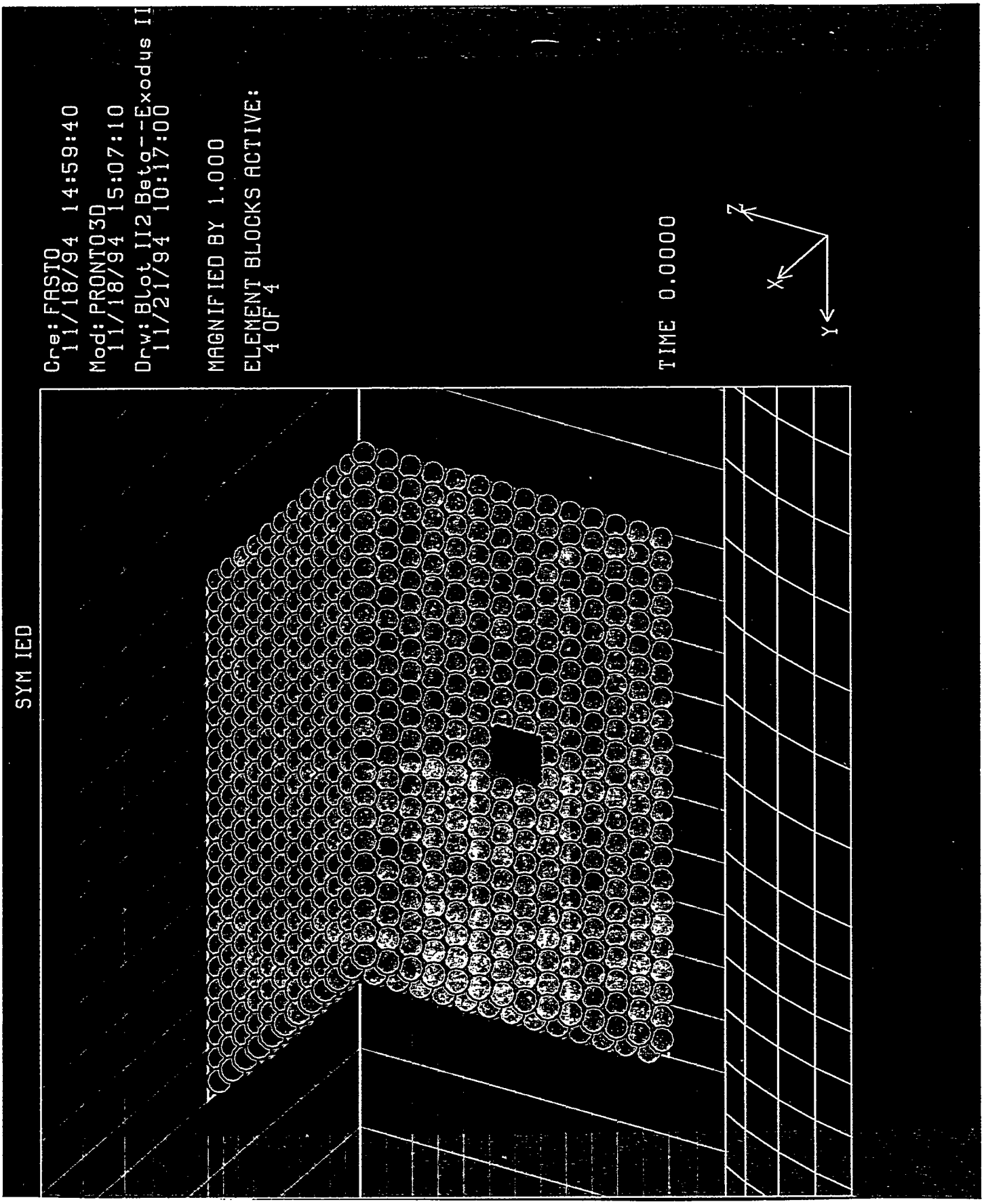

Figure 4.2 Close-up of the SPH region for the submerged cylinder problem.

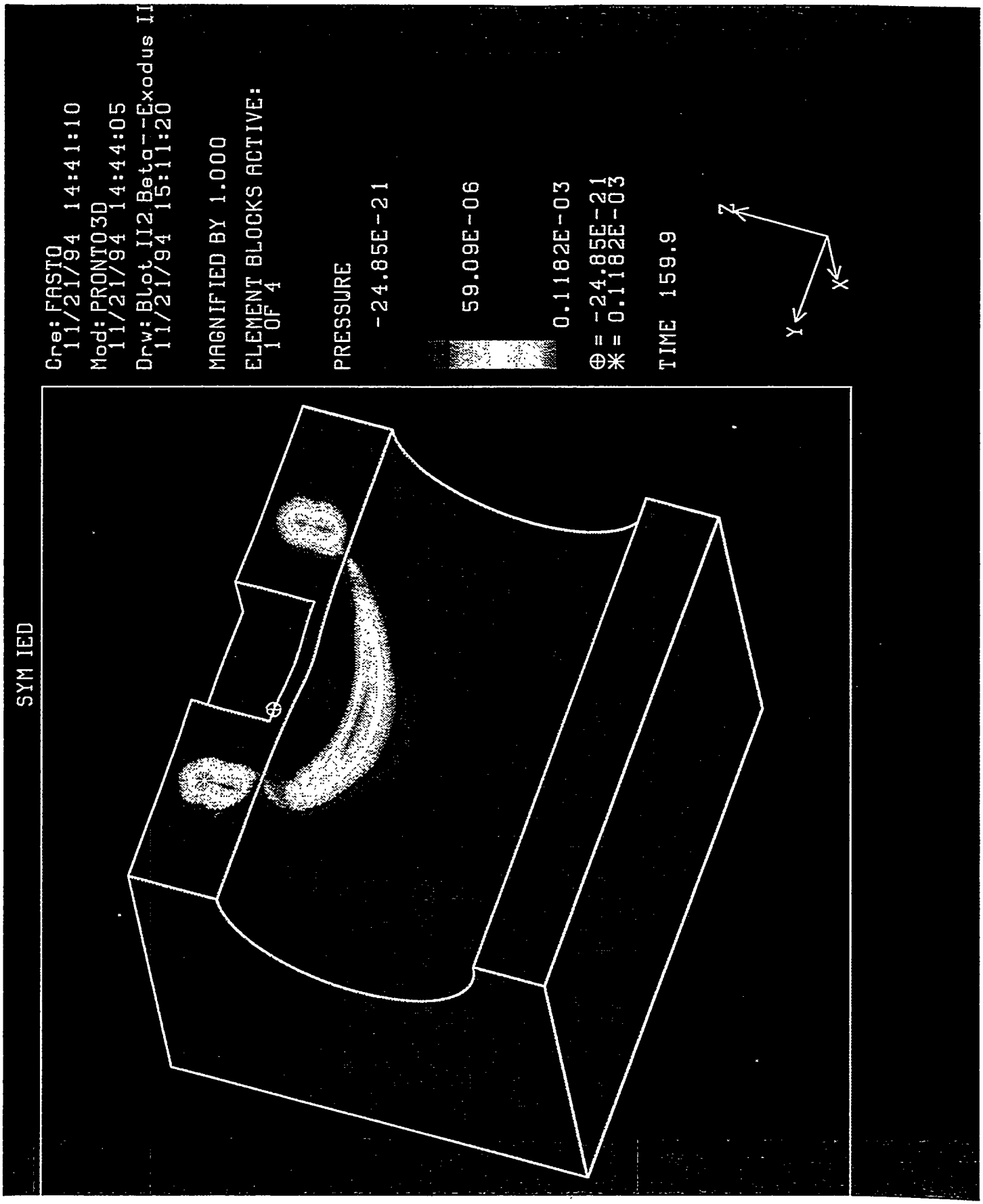

Figure 4.3 Pressure pulse from detonation of the explosive charge. Pressure units in Mbar

Cylinder Dimensions:

Length 0.92 m, Diameter 0.46 m, Thickness 0.0048 m

Charge: Pentalite, 15 gm, Depth 0.07 m

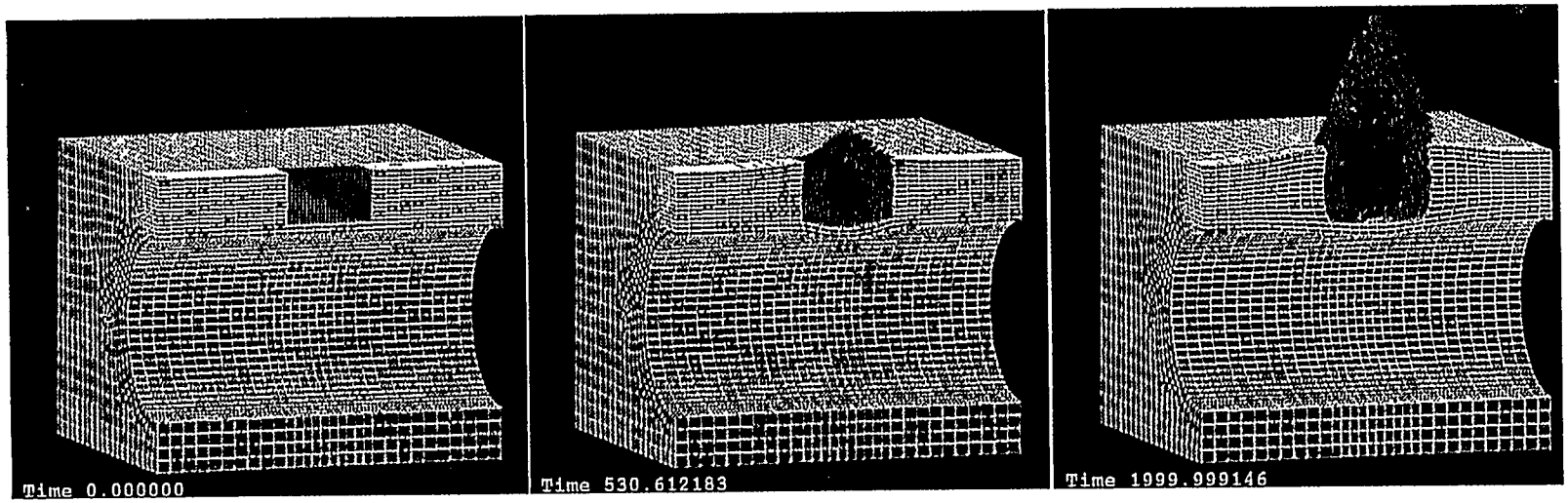

Figure 4.4 Material deformation plots. Times in microseconds.

5. Deep Explosion Beneath a Flat Plate

The final test involves the detonation of a deep charge beneath a flat steel plate. The plate is circular in shape, 70 inches in diameter and 1 inch thick, with a 1 foot diameter, 6 inch thick aluminum plug bolted into the center. The explosive charge is 10 gm of CH6, placed 5.5 inches below the center of the plate. The entire assembly is at a depth of 167 feet. This test is representative of a series of tests known as Seneca Lake[16]. Figure 5.1 shows the initial three-dimensional mesh for the problem. The entire problem is represented by hexagonal finite elements, except for the explosive and water directly beneath the plate. This is treated with SPH, shown in close-up in Figure 5.2. For this problem gravity was included, and the initial pressure in the water was initialized to a depth-dependent value so that the pressure field in the water was in equilibrium with the acceleration of gravity. The initial pressure field in the water is shown in Figure 5.3, with pressure units in Mbar. The initial pressure at the depth of the plate is about 6 bar. The water boundary at depths below the charge location was placed 2000 m away from the charge to preclude signals reflecting from the boundary back to the plate during the 15 ms duration of the event. The pressure was maintained by use of a no-displacement boundary condition at this location. To allow for vertical plate movement, an applied pressure boundary condition was used on the upper horizontal surfaces.

The propagation from the SPH region to the finite-element water of the initial pressure wave due to detonation of the explosive is shown in Figure 5.4 at a time 0.9 ms after the detonation. Only the finite element water and not the SPH region or the metal plates is shown in the figure. A series of snapshots of the explosive bubble at various times during the calculation is shown in Figure 5.5, in which the color of the SPH region is based on density. In the actual tests, the bubble is observed to expand until it begins to interact with the plate, and by 10 ms the upper portion of the bubble has risen to contact and attach to the plate, producing a flat upper boundary. Around 12 ms the bubble begins to collapse from the bottom, producing a jet which impacts on the plate at about 15 ms. The figure shows that these events are not seen in the calculation. The bubble does not attach to the plate and begins to collapse uniformly near its original position. Also, the boundary between the SPH water and the finite element water shows an hourglass shape at late times due to the flow of the water apparently being too weak near the plate. This is indicative of excessive friction at the plate-water interface, which likely also affects the bubble motion in this region. However, it is clear that it is not reasonable to expect the calculations to be able to capture both the strong fluid-structure shock wave interactions present at early times in the calculation and also the late time effects due to acceleration of gravity and bubble buoyancy, without some special effort to mitigate numerical effects present not only in this method, but in most (all?) others as well. In the centimeter-gram-microsecond system of units which is most convenient for shock calculations, normal accelerations during an event are of the order of unity, while the acceleration of gravity is of order 10^{-9}. While most would

consider a few percent to be reasonable accuracy in an explicit dynamics simulation of the type considered here, no one would expect accuracy in the 9th significant digit. It is clear that numerical effects such as artificial viscosity, hourglass viscosity, and minor inaccuracies will swamp the late time phenomena seen in actual tests, and the ability to accurately model these phenomena in the same calculation which accurately models the early shock phenomena will require extensive method development and fine tuning of numerical artifacts. An additional concern is the amount of computer time required to reach such late times with an explicit dynamics calculation. The small spatial dimensions present in the problem limit the time step so that tens or hundreds of thousands of time steps may be required to reach the desired problem time, requiring tens of hundreds of hours of CPU time. Some sort of implicit method (with no explicit time step limitation) or perhaps an incompressible treatment might be more efficient for the intermediate stages of a problem such as this.

It might also be noted that the calculation shown above was done in three dimensions, even though the experiment is conceptually two-dimensional and axisymmetric. The axisymmetric option developed for PRONTO/SPH has been extensively tested and compared to analytic solutions in simple geometries where analytic solutions are known. The method clearly works and has been shown to produce correct results in these situations, as well as in the axisymmetric results shown previously. However, SPH has a peculiar difficulty in axisymmetric calculations which does not occur with gridded methods. Although the method is correct given a reasonable distribution of particles, in certain anomalous circumstances a single particle can get into trouble with the singularity at the symmetry axis. Since a single particle's density is proportional to radius due to the fact that a particle represents a torus of revolution in axisymmetry, particles which stray too near the axis can have their density and thus pressure increase to unreasonable levels. This would not occur with a gridded method, since even if a single element experienced a density increase as it neared the axis, the internal pressure in the element would cause it to expand, thereby reducing the pressure. However, a single particle has no degrees of freedom and cannot expand to reduce the density. Extreme pressures can thus be generated which destroy the calculation. An example is shown in Figure 5.6 which shows the end-on impact of two cylinders. The material jets outward at the impact plane, whose normal is along the symmetry axis. The calculation proceeds normally until at late times a particle drifts too near the symmetry axis, producing a large pressure which then drives the other particles from its vicinity, effectively blowing a hole in the problem. This phenomenon does not occur in all axisymmetric calculations, but does prevent certain calculations from proceeding to completion.

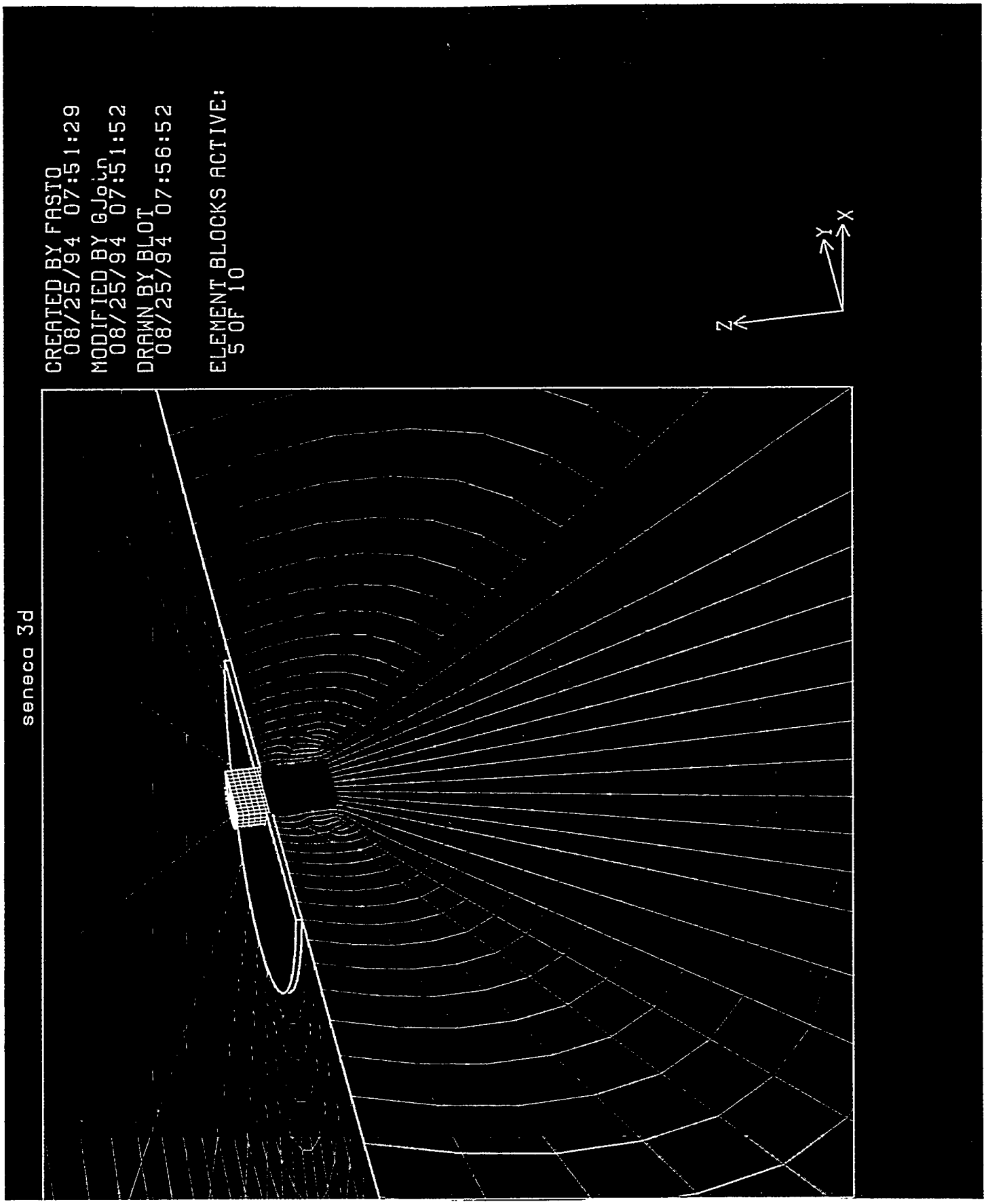

Figure 5.1 Mesh for the flat plate problem.

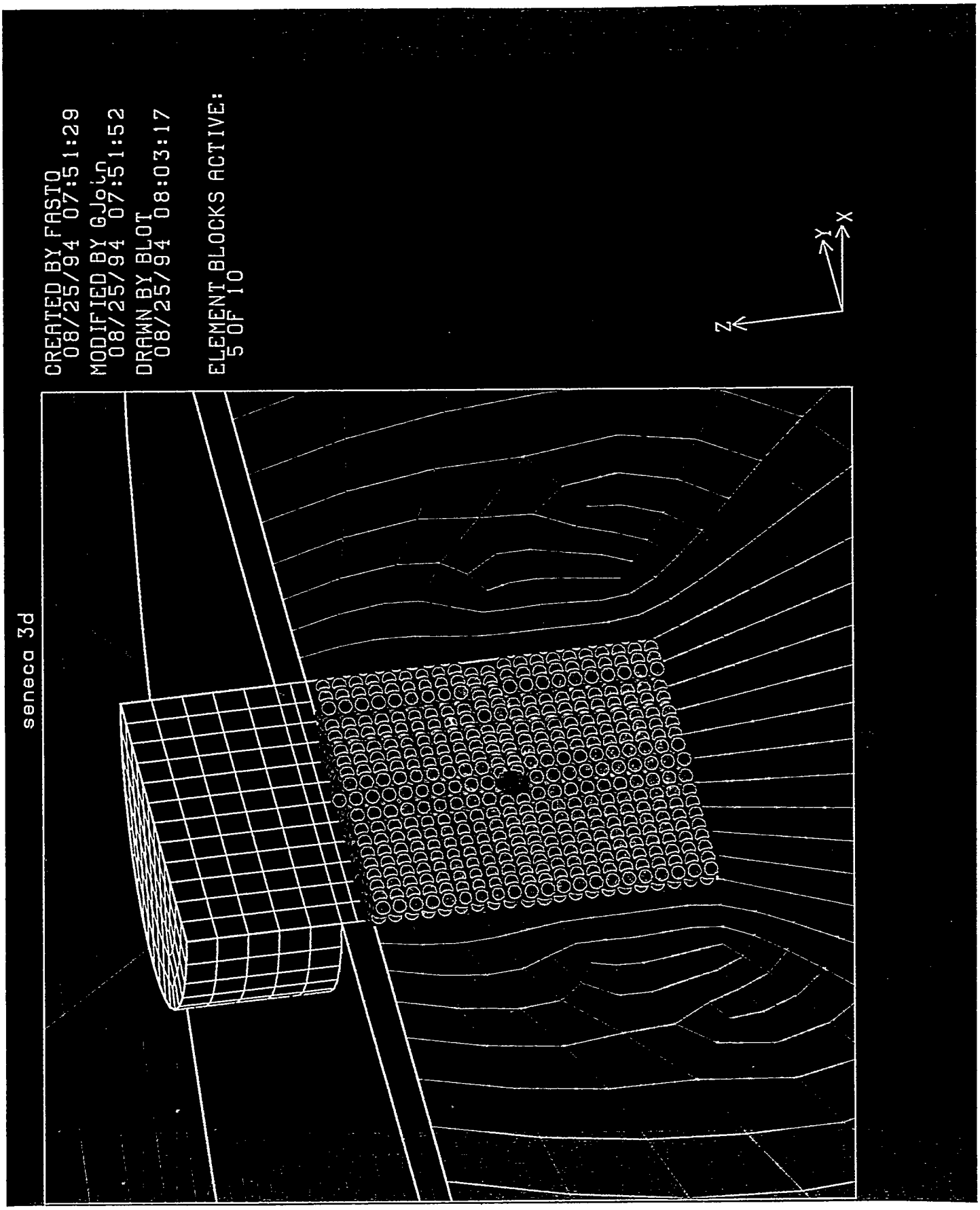

Figure 5.2 Close-up of the SPH region for the flat plate problem.

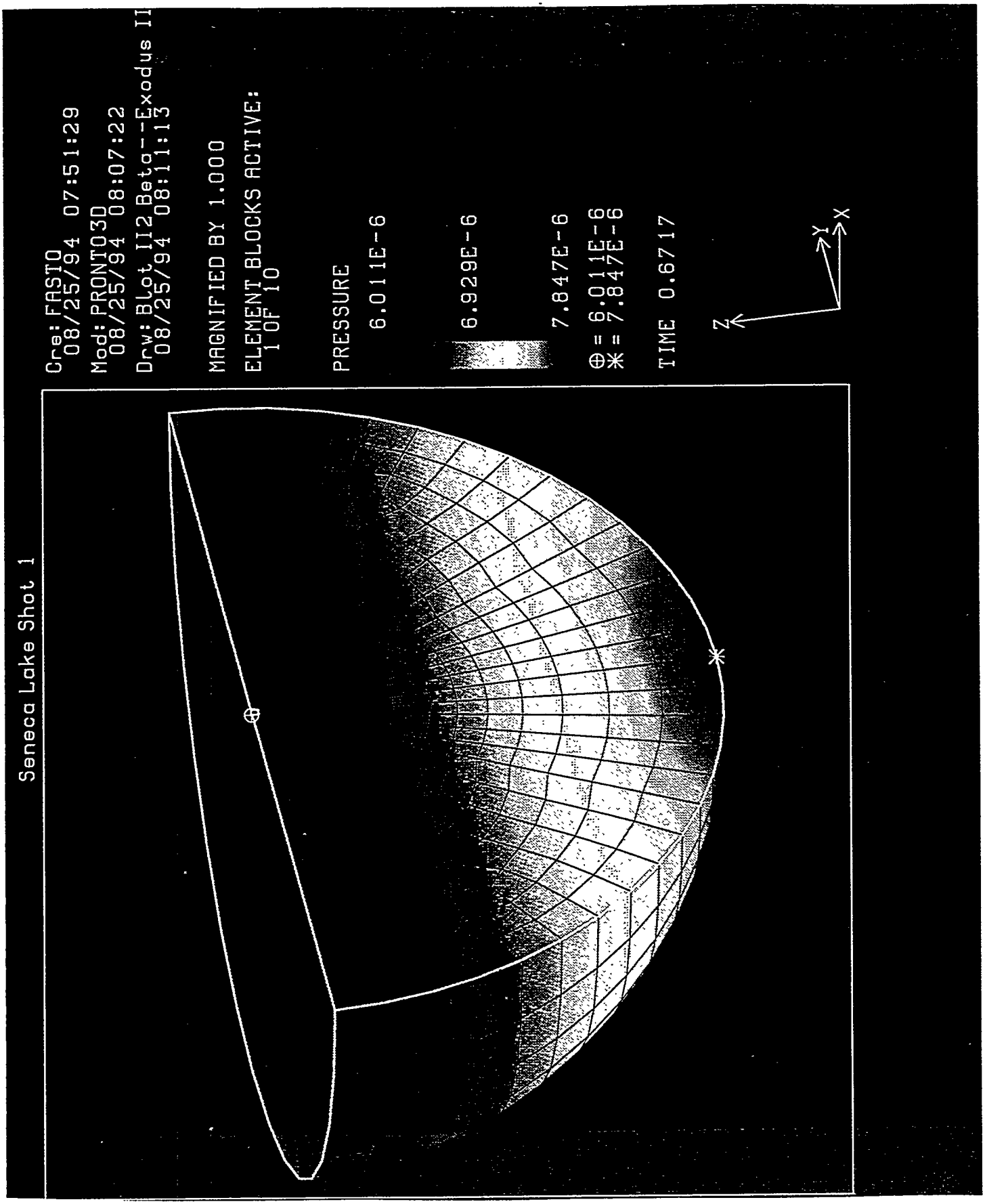

Figure 5.3 Initial pressure field in the water in equilibrium with the acceleration of gravity. Pressure units in Mbar.

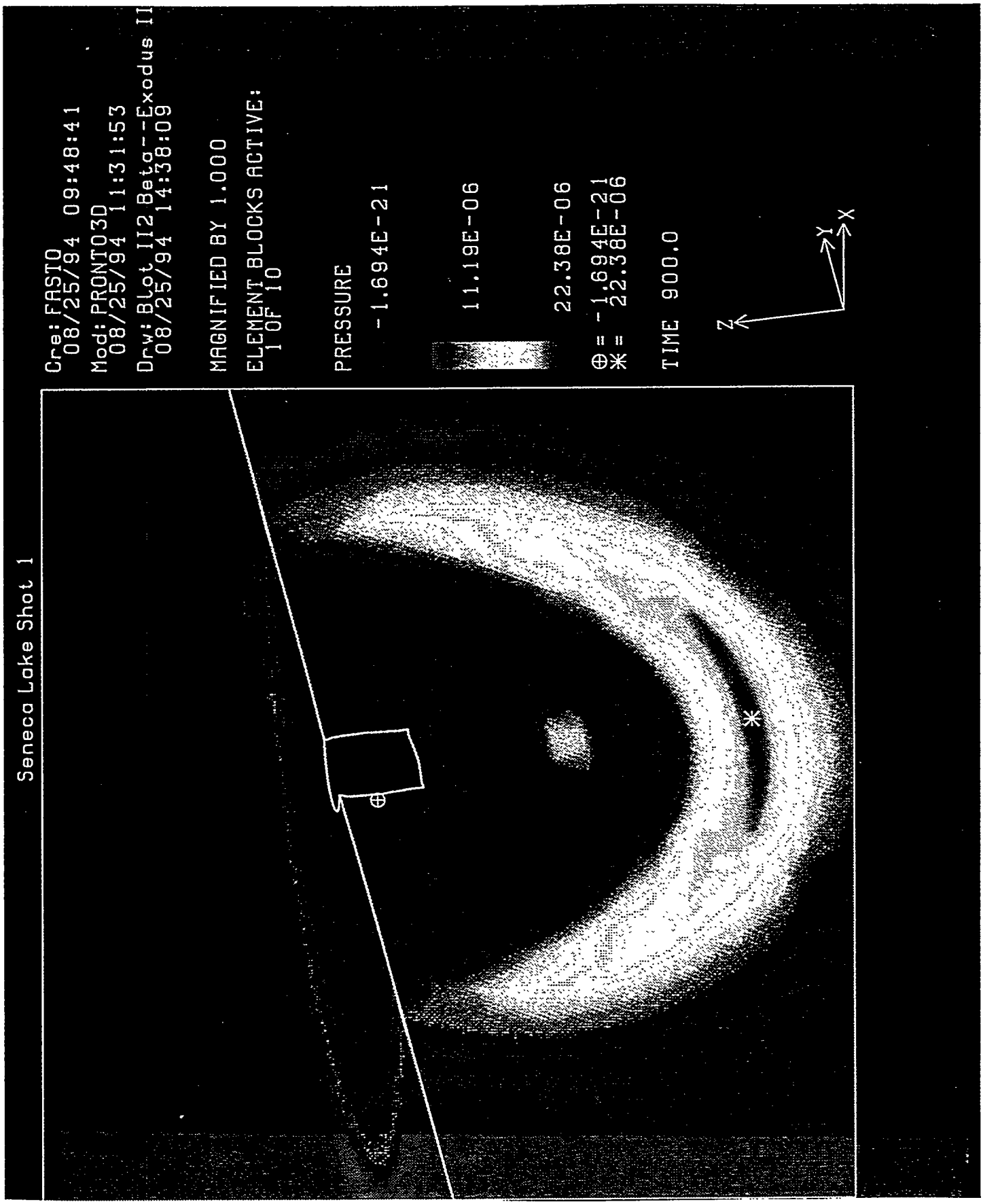

Figure 5.4 Pressure pulse from detonation of the explosive charge. Pressure units in Mbar

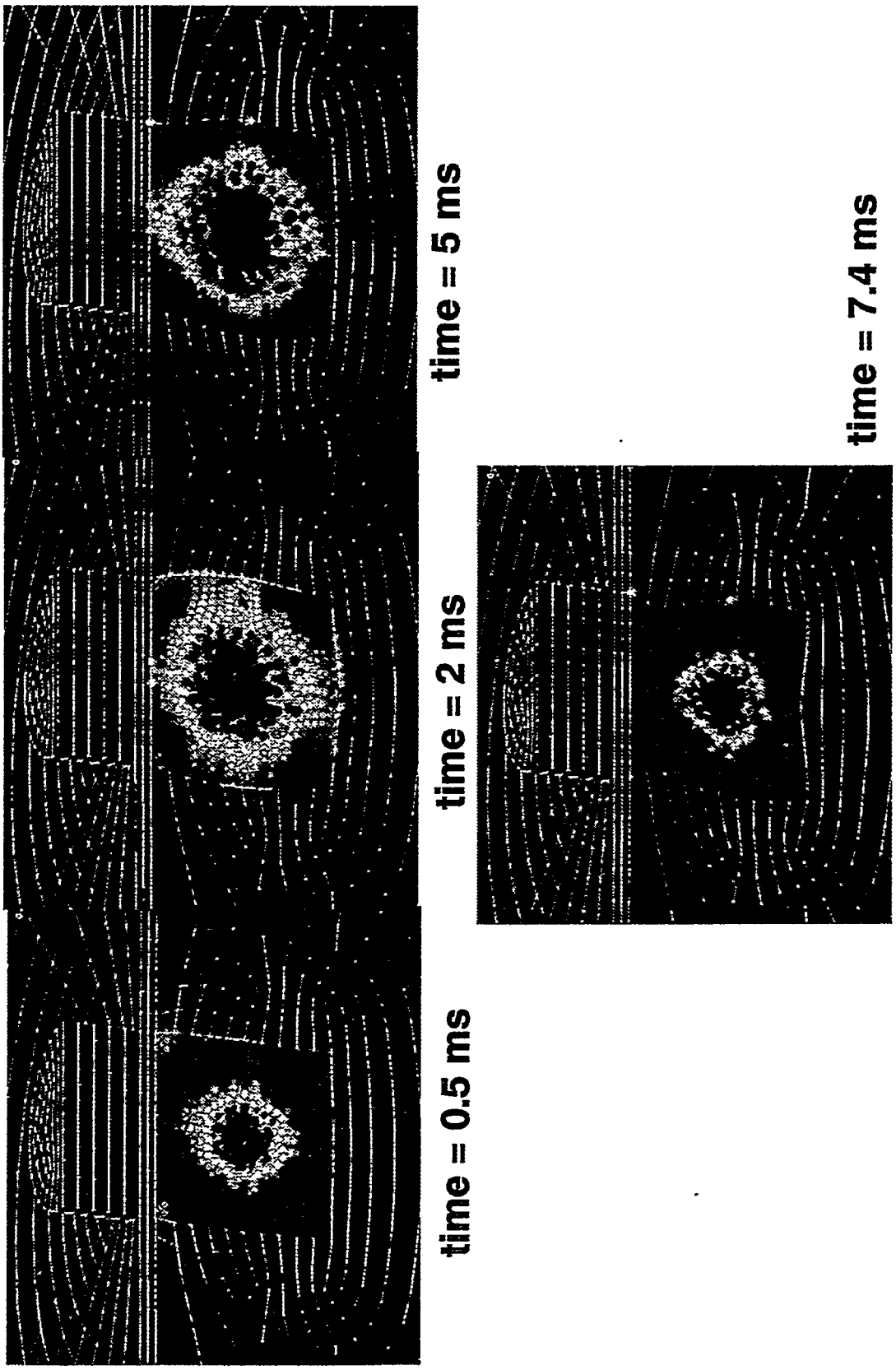

Figure 5.5 Material deformation plots. Color based on density in the SPH region.

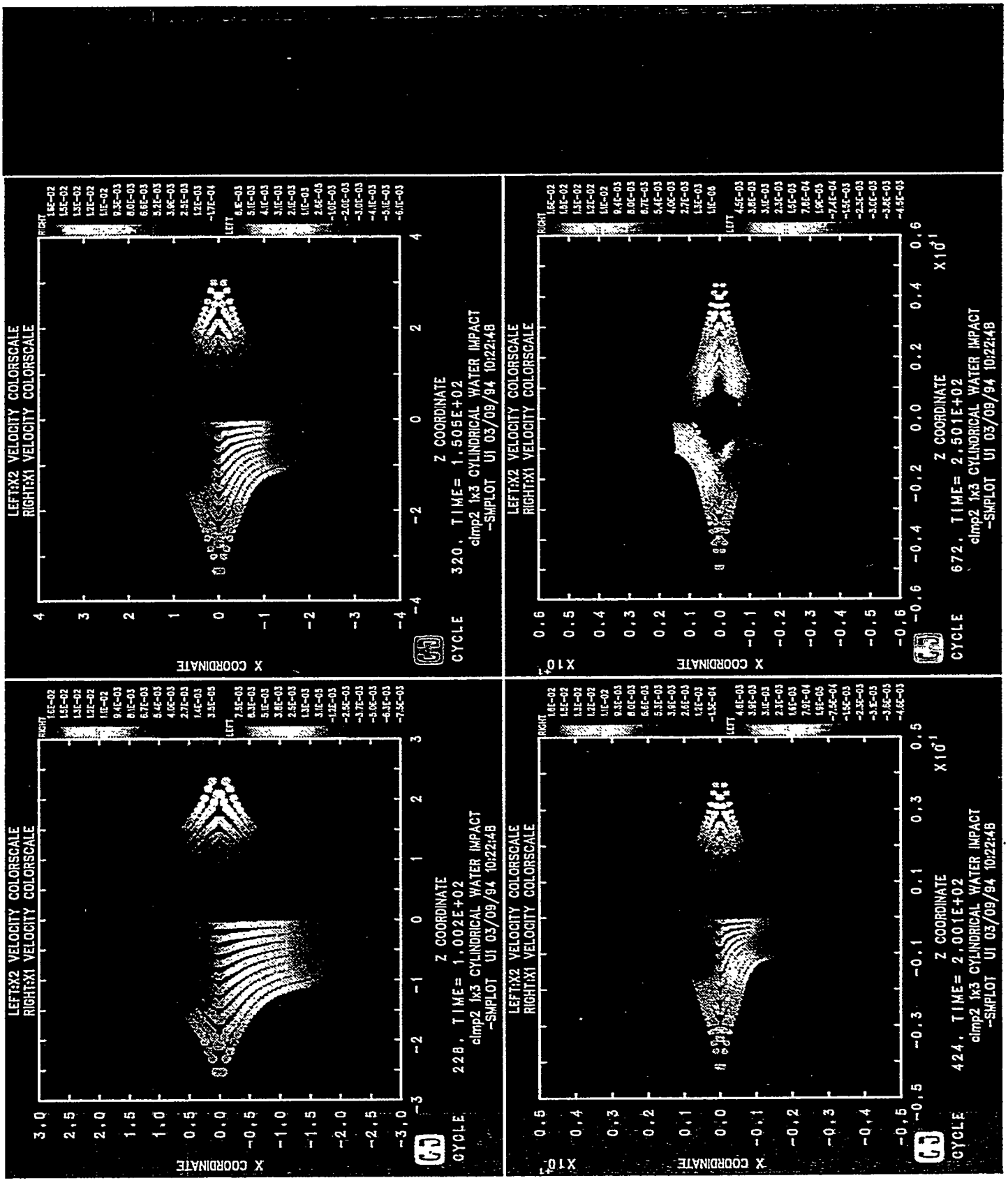

Figure 5.6 End-on impact of two cylinders illustrating the axisymmetric singularity.

6. Conclusion

Smoothed particle hydrodynamics (SPH) is a gridless Lagrangian technique which shows potential for detailed analysis of high deformation events which are not well handled at present by either Eulerian or standard Lagrangian techniques. In principle, the method should be able to overcome both the diffusion problems associated with Eulerian methods and the grid distortion associated with Lagrangian methods. The name 'smoothed particle hydrodynamics' is misleading, since the particles are actually interpolation points, and the method is not hydrodynamic, since inclusion of full stress and strain tensors is easily accomplished. The apparent strength of SPH is the calculation of spatial gradients by a kernel approximation method which does not require connectivity of the particles and should be able to treat arbitrary deformations. In the present study, the SPH algorithm has been subjected to detailed testing and analysis to determine its applicability to underwater explosion problems involving fluid-structure and shock-structure interactions.

The sample problems show that PRONTO/SPH is well-suited for transmission of loads from underwater explosions to nearby structures, including the permanent deformation of thin walled structures due to these explosions. However, it is clear that it is not reasonable to expect the calculations to be able to capture both the strong fluid-structure shock wave interactions present at early times in the calculation and also the late time effects due to acceleration of gravity and bubble buoyancy. Numerical effects such as artificial viscosity, hourglass viscosity, and minor inaccuracies swamp these very late time phenomena which are due to physical forces and effects which are many orders of magnitude more subtle than those involved in the early parts of the event. The ability to accurately model these late-time phenomena in the same calculation which accurately models the early shock phenomena will require extensive method development and fine tuning of numerical artifacts. Also, the amount of computer time required to reach such late times with an explicit dynamics calculation is a major concern. The small spatial dimensions present in the problem limit the time step so that hundreds of thousands of steps may be required to reach the desired problem time, requiring tens or hundreds of hours of CPU time. An implicit method with no explicit time step limitation, or perhaps an incompressible treatment, might be more efficient for some parts of the problem. Although the current investigation has revealed areas in SPH (as well as most other numerical methods) that need improvement if late-time gravitational effects are to be modeled, the potential of the method in the area of large deformation Lagrangian calculations is very real.

References

1. L. B. Lucy, "A Numerical Approach to the Testing of the Fission Hypothesis," *A. J.* **82** (1977), 1013-1024.

2. R. A. Gingold and J. J. Monaghan, "Kernel Estimates as a Basis for General Particle Methods in Hydrodynamics," *J. Comp. Phys.* **46** (1982), 429-453.

3. J. J. Monaghan, "Why Particle Methods Work," *SIAM J. Sci. Stat. Comput.* **3** (1982), 422-433.

4. J. J. Monaghan, "Particle Methods for Hydrodynamics," *Comput Phys. Rep.* **3** (1985), 71-124.

5. J. J. Monaghan, "An Introduction to SPH," *Comp. Phys. Comm.* **48** (1988), 89-96.

6. L. D. Cloutman, "Basics of Smoothed Particle Hydrodynamics," Lawrence Livermore National Laboratory report UCRL-ID-103698, 1990.

7. L. D. Cloutman, "An Evaluation of Smoothed Particle Hydrodynamics," T *proceedings of The NEXT Free-Lagrange Conference*, Jackson Lake Lodge, Moran, Wyoming, June 3-7, 1990.

8. W. Benz, "Smooth Particle Hydrodynamics: A Review", in The Numerical Modeling of Stellar Pulsation, ed. J. R. Buchler (Dordrecht: Kluwer), (1990), 269.

9. J. W. Swegle, S. W. Attaway, M. W. Heinstein, F. J. Mello, and D. L. Hicks, "An Analysis of Smoothed Particle Hydrodynamics", Sandia National Laboratories Report, SAND93-2513,1994.

10. L. M. Taylor and D. P. Flanagan, "PRONTO 2D - A Two-Dimensional Transient Solid Dynamics Program", Sandia National Laboratories Report, SAND 86-0594, 1987.

11. H. Huang, "Transient Interaction of Plane Acoustic Waves with a Spherical Elastic Shell," *J. Acoust. Soc. Amer.* **45** (1969), 661-670.

12. Peizhen Zhang and Thomas L. Geers, "Excitation of a fluid-filled, submerged spherical shell by a transient acoustic wave," *J. Acoust. Soc. Amer.* **93** (1993), 696-705.

13. R. H. Cole, **UnderWater Explosions**, Dover Publications, 1965.

14. J. W. Swegle, "TOODY IV - A Computer Program for Two-Dimensional Wave Propagation", Sandia National Laboratories Report, SAND78-0552,1978.

15. Charles McClure, "Preliminary Report on Explosive Field Tests in Support of the Hull Deformation/Rupture Study", NSWC Report NSWCDD/TN-93/94, 1993.

16. Robert Thrun, John F. Goertner, and Gregory S. Harris, "Underwater Explosion Bubble Collapse Against a Flat Plate. 1992 Seneca Lake Test Series Data Report", NSWC Report NSWCDD/TR-92/482, 1993.

DISTRIBUTION:

S. Atluri
Center for the Advancement of
Computational Mechanics
School of Civil Engineering
Georgia Institute of Technology
Atlanta, GA 30332

E. B. Becker
Department of Aerospace Eng. and
Engineering Mechanics
The University of Texas at Austin
Austin, TX 78712-1085

T. Belytschko
Department of Civil Engineering
Northwestern University
Evanston, IL 60201

Dave Benson
Department of Applied Mechanics
and Engineering Sciences
University of California San Diego
La Jolla, CA 92093

Naury K. Birnbaum
Century Dynamics Incorporated
7700 Edgewater Dr., Suite 626
Oakland CA 94621

Gregory Clifford
Cray Research Park
655E Lone Oak Drive
Eagan, MN 55121

Peter Cundall
ITASCA Consulting Group, Inc.
1313 Fifth Street, S.E.
Minneapolis, MN 55414

Carl Dyka
Naval Research Lab
Materials Science & Technology
Building 28, Code 6386
4555 Overlook Avenue SW
Washington, DC 20375-5000

R. Douglas Everhart
Battelle
505 King Avenue
Columbus, OH 43201-2693

D. P. Flanagan
Hibbitt, Karlsson & Sorrensen, Inc.
100 Medway St.
Providence, RI 02906

Arlo Fossum
RE/SPEC Inc.
Box 725
Rapid City, SD 57709

Gerry Goudreau
Methods Development Group
Mechanical Engineering Department
Lawrence Livermore National Lab
Livermore, CA 94550

Jerome B. Johnson
USACRREL
Building 4070
Ft. Wainwright, AK 99703

Sheldon Jones
Kaman Sciences
P.O. Box 7463
Colorado Springs, CO 80933-7463

David W. Keck
CONVEX Computer Corporation
P.O. Box 833851 M.S. MAR
Richardson, TX 75083-3851

Raymond D. Krieg
Engineering Science and Mechanics
301 Perkins Hall
University of Tennessee
Knoxville, TN 37996-2030

Hans Mair, Code R14
Naval Surface Warfare Center
10901 New Hampsure Ave.
Silver Spring, MD 20903-5000

Loren K. Miller
Goodyear Technical Center
P.O. Box 3531
Akron, OH 44309-3531

S. Nemat-Nasser
Department of Applied Mechanics
and Engineering Sciences
University of California San Diego
La Jolla, CA 92093

J. T. Oden
Department of Aerospace Eng.
and Engineering Mechanics
The University of Texas at Austin
Austin, TX 78712-1085

Allan B. Pifko
Grumman Corporate Technology
Bethpage, NY 11714-3580

Mark Rashid
Department of Civil &
Environmental Engineering
University of California
Davis, CA 95616-5294

J. S. (Gus) Rice
Caterpillar Inc. Technical Center
Division 927
P.O. Box 1875
Peoria, IL 61656-1875

Steven F. Rieco
POD Associates, Inc.
2309 Renard Pl, Suite 201
Albuquerque, NM 87106

R. G. Sauvé
Mechanical Research Department
Ontario Hydro
700 University Avenue C26
Toronto, Ontario M5G 1X6
Canada

L. M. Taylor
Hibbitt, Karlsson & Sorrensen, Inc.
100 Medway St.
Providence, RI 02906

2 Air Force Institute of Technology
Dept. of Mathematics & Statistics
2950 P Street
Attn: Michael Stoecker
Dave Fulk
Wright-Patterson Air Force Base
Dayton, OH 45433-7765

Gordon Johnson
Alliant Tech Systems , Inc.
(MN 11-2925)
600 2nd St. NE
Hopkins, MN 55343

Marv Alme
Alme and Associates
2 Stevens Forest Prof. Center
9650 Santiago Road
Columbia, MD 21045

Ted Carney
Applied Research Associates
4300 San Mateo Blvd. NE
Suite A-220
Albuquerque, NM 87110

3 Batelle
505 King Avenue
Attn: Mike Fisher
Doug Everhart
Chuck Hargraves
Columbus, OH 43201-2693

2 Cray Research, Inc.
6565 Americas Parkway, NE
Suite 830
Attn: Phil Campbell
Dave Shirley
Albuquerque, NM 87110

Lou Baker
Dagonet Software
2904 La Veta Dr. NE
Albuquerque, NM 87110-3110

Lawrence Livermore National Lab
Bill Hoover
MS L-794
P. O. Box 808
Livermore, CA 94550

15 Darrell L. Hicks
Michigan Tech. University
Math Department
Houghton, MI 49931

Joe Monaghan
Monash University
Mathematics Department
Clayton, Vic. 3168
Australia

Larry Libersky
NM Institute of Mining and Tech.
Center for Explosives Tech. Research
Socorro, NM 87801

5 Phillips Laboratory
PL/WSSD
Kirtland Air Force Base
Attn: Charles Luehr
David Medina
James Ninter
Brad Smith
Firooz Allahdadi
Albuquerque, NM 87117

Willy Benz
University of Arizona
Steward Observatory
Tucson, AZ 85721

Rita Smith
University of New Mexico
Dept. of Chemical/Nuclear Engin.
Farris Engineering Center
Albuquerque, NM 87131-1341

FCDNA
Attn: FCTTS/Phil Randles
1680 Texas Street SE
Kirtland AFB, NM 87117-5669

12 Los Alamos National Laboratory
Los Alamos, NM 87545
Attn:
J. P. Hill, WX-11, MS C931
B. L. Holian, T-12, MS B268
D. A. Rabern, MEE-4, MS G787
P. S. Follansbee, MS G756
D. Mandell, X-3, MS F663
R. F. Davidson, N-6, MS K557
N. L. Johnson, T-3, MS B261
J. K. Dienes, N-6, MS K557
C. A. Anderson, MS J576
M. W. Lewis, MEE-4, MS G787
C. Wingate, MS F645
B. Stellingwerf, MS F645

Sandia Internal:

	MS1187	1271	George Allshouse
	MS1184	1239	Frank Dempsey
	MS0321	1400	Ed Barsis
	MS0441	1425	P. L. Stanton
	MS0819	1431	Mike McGlaun
	MS0820	1432	Paul Yarrington
	MS0820	1433	M. E. Kipp
	MS0439	1434	David Martinez
	MS0841	1500	P. J. Hommert, Actg.
	MS0827	1502	P. J. Hommert
	MS0833	1503	J. H. Biffle
	MS0828	1504	E. D. Gorham
	MS0827	1511	J. H. Biffle, Actg.
	MS0827	1511	Jim Schutt
	MS0834	1512	A. C. Ratzel
	MS0835	1513	R. D. Skocypec
	MS0826	1514	W. L. Hermina
	MS0825	1515	W. H. Rutledge
	MS0836	1516	C. W. Peterson
16	MS0443	1517	H. S. Morgan & Staff
15	MS0437	1518	R. K. Thomas & Staff
5	MS0437	1518	S. W. Attaway
25	MS0437	1518	J. W. Swegle
	MS0336	1707	Kim Mahin
	MS0515	2561	S. T. Montgomery
	MS0660	2861	Randall Lober
	MS0457	5600	Dennis Hayes
	MS0574	5941	John Schamaun
	MS0724	6000	Dan Hartley
	MS0751	6117	Dale Preece
	MS1325	6313	Joseph Jung
	MS1143	6500	James Rice
	MS1145	6514	Jim Fisk
	MS1145	6514	Joel Miller
	MS9214	8117	William Mason
	MS9401	8702	Bill Robinson
	MS9043	8743	George Johnson
	MS9042	8741	Juanita Benson
	MS9042	8741	Michael Chiesa
	MS9042	8742	Jay Dike
	MS9042	8742	Paul Jin
	MS9042	8742	Bruce Kistler
	MS9042	8742	Khanh Trinh
	MS9042	8742	Paul Nielan
	MS9043	8743	Melvin Callabresi
	MS9043	8743	Douglas Bammann
	MS9043	8743	Lee Bertram
	MS9043	8743	Mark Horstemeyer
	MS9043	8743	James Lathrop
	MS9043	8743	Arthur Ortega
	MS9043	8743	Vincent Prantil
	MS9043	8745	William Winters
	MS0974	9421	Jeanne Ramage
5	MS0899	13414	Technical Library
	MS0619	12615	Print Media
2	MS0100	7613-2	Document Processing for DOE/OSTI
	MS9018	8523-2	Central Tech Files